International Journal of Engineering Research & Technology (IJERT)
ISSN: 2278-0181
Vol. 6 Issue 02, February-2017

# Comparison of Experiment Data to Model of Shaker Separator

Vidya Raja
Schlumberger Technology Corporation,
Katy, TX 77493

Saeid Ghaniyari-Benis
Department of Chemical and Biomolecular Engineering,
The University of Akron,
Akron, Ohio 44325

George G Chase*
Department of Chemical and Biomolecular Engineering,
The University of Akron,
Akron, Ohio 44325

***Abstract*—Shakers are used to separate sand particles from process fluids such as drilling muds. A continuum model of the cake is discussed and compared to experimental data from a full scale shaker. The model accounts for the non-Newtonian yield stress rheology of the drilling mud. The model calculations show that there is a good agreement between the model and the experimental data. The model calculates the cake thickness profile that is expected from the theory.**

***Keywords—: Filter cake, shale shaker, vibrating screen, drilling fluids, yield stress***

## I. INTRODUCTION

Shakers are used to separate coarse particles of sand and shale from liquid-solid slurries (muds) produced during petroleum drilling operations. The slurry enters the shaker onto a vibrating screen on which the solid particles form a cake and the liquid passes through. The screen is vibrated to enhance the liquid flow rate and to transport the particulate cake off of the screen [1, 2]. The liquid phase is often recycled back to the drilling operation. The liquid phase may be an aqueous or organic engineered fluid with a dispersion of micron sized clays or synthetic particles that provide the liquid with rheological properties designed to enhance the transport of the coarse drilling particles from the drilling head to the top of the borehole. The liquid phase also lubricates and cools the drilling head.

The flow capacity of a shaker is determined by factors including rheology of the liquid, the size and concentration of the coarse particles, the screen properties, and the operating parameters [3, 4]. Few publications discuss models of shaker performance. Hoberock [5, 6] developed a model based on open-channel hydraulics for screens inclined downward. Frictional drag forces of the drilling mud on the side walls of the flow channel were balanced with the flow through the screen to determine the depth of the free surface of the mud as it flowed onto and across the screen. Hoberock recognized that the screen maximum liquid flow capacity is limited by the flow through the screen in the absence of the cake. Hoberock also applied yield stress rheology of the mud flow in the channel. The model did not apply to shakers with upward inclined screens and it did not account for the formation of the cake on the screen. Others established empirical relationships to predict screen flow rates [7-9] . Weibing et al, [10] applied two-phase flow theory to model the motions of the suspended particles in the mud and developed a model to predict the solids conveyance velocity across the screen.

The complexity of the shaker limits the use of the available models. Improvements are needed for optimizing and controlling shaker performance. The ideal model should account for enough of the underlying physics to give useful prediction but not be intractable or too computationally intensive.

A model for the formation of the cake on a shaker was reported but had limited experimental data for comparison and was limited to Newtonian fluids [11]. Here the prior model is improved and model calculations are compared with experimental data from a full-scale Mongoose PT shale shaker (M-I SWACO, A Schlumberger Company, with an API 140 screen). The results show under certain conditions the model is in good agreement with the experimental data. More work will be needed to further improve the model.

## II. EXPERIMENTS

Three experiments were conducted on the full scale shaker with variation in maximum screen acceleration, all other parameters were held constant or nearly constant. The screen acceleration primarily affected the velocity at which the cake traversed across the surface of the screen. The experimental data are listed in Table 1. The maximum accelerations (indicated as number of gravities, $G_{max}$) were a function of the frequency and motor settings and were measured using an accelerometer.

The mud was prepared as a mixture of water, clay, and sand in a large stirred tank. The mud was pumped into the shaker at a steady rate that gave a reasonable mud depth on the screen. The liquid phase (water and clay suspension) was separated from the cake of coarse particles by the shaker operation. The exiting liquid phase and the exiting cake were recycled back to the supply tank to replenish the mud for extended operations. The observed mud depth ranged about 0.1 to 0.2 m but was turbulent and inaccurate to measure. The cake velocity was determined by observing the movement of a marker on the surface of the cake. The deck angle was 3 degrees for all three experiments.

The coarse particles (QUIKRETE All-Purpose Sand) that formed the cake varied in size from about 100 microns to 2 mm and had an average size of 0.3 to 0.4 mm as determined by a sieve analysis. The colloidal clay particles (Bentonite clay and barite) ranged from 0.1 to 20 microns (measured with a Coulter Analyzer) with an average size of 3 to 4 microns. The clay particles did not contribute significantly to the cake, but did affect the rheology of the liquid.

The clay and sand had approximate intrinsic densities of 3400 and 2600 kg m-3 and water was assumed to have a density of 998 kg m-3. The measured bulk density of the liquid phase listed in Table 1 was used to calculate the volume fraction of clay in the liquid phase. The clay volume fraction was used to estimate the plastic viscosity,$\mu_o$, and the yield stress, $\tau_o$, of the liquid phase using relations from literature [12]

Packed beds are known to have porosities ranging from 0.3 for dense packing to 0.45 for loose packing [13]. Since the cake was formed by settling the latter value was assumed for the experiments. However, Raja [14] showed that vibrated bed porosities can range up to 0.55.

The model input parameters in Table 1 formed the base case for the calculations. The observed cake velocity and inlet mud height were also input into the computer model. The liquid flow rate, cake height, and length of mud across the screen were observed in the experiments.

## III. MODEL CALCULATIONS

In this model the air-mud interface is horizontal from the inlet to where it meets the cake on the surface of the inclined screen. The mud flows into the shaker at the inlet at $x = 0$ and forms a pool of depth $h_o$ above the screen as indicated in Fig.1. As the liquid phase flows through the screen the coarse particles in the mud collect on the screen and form a cake. The vibrations of the screen cause the cake to traverse across the screen while the liquid phase exits the bottom of the screen. The movements of the screen are small compared to the dimensions of the cake and mud and are not explicitly used in the model.

Based on mass continuity, the rate of change of the cake height $h_c$ on the screen depends on the liquid volume fractions in the mud ($\varepsilon^m$) and cake ($\varepsilon^c$), on the liquid face velocity through the cake ($V$), and on the velocity of the cake moving on the screen ($v_x^c$) by the equation (see Appendix for derivation of equations)

$$\frac{dh_c}{dx} = -\left(\frac{1-\varepsilon^m}{\varepsilon^m-\varepsilon^c}\right)\frac{V}{v_x^c} \quad (1)$$

The superscript notation c and m indicate the cake and mud domains. The liquid velocity is determined at each position x by solving the momentum balance

$$\left(\frac{F_z^c}{\varepsilon^c}h_c + \frac{F_z^{scr}}{\varepsilon^{scr}}h_{scr}\right) + [\rho^m(h_m - h_c) + \rho^L(h_c + h_{scr})]g = 0 \quad (2)$$

where the drag forces $F_z^c$ and $F_z^{scr}$ are functions of $V$.

The revised model applies a modified Ergun Equation for a yield stress liquid flowing through a packed column [15]. Equation (2) relates the static pressure head of the mud, cake, and screen to the drag forces. The drag forces are related through friction factors of a packed column [16] to the velocity, $V$. The model includes conditions that must be satisfied for flow to occur due to the yield stress.

The flow rate, cake height, and the length of the mud on the screen were calculated with the model equations and data in Table 1. A comparison of the calculated results are summarized in Table 2. For each experiment the observed experiment values listed in the Table 1 row and the calculated flow rate, cake height, and wetted cake length (Q, $h_c$, and L) values are listed in the Calculated column. The shaded values in Table 2 are those that were

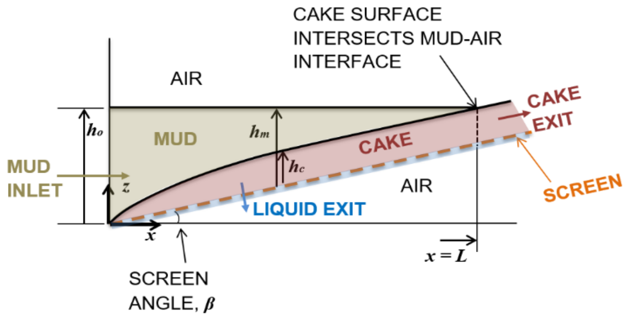


Figure 1. Diagram of vibrating screen inclined at angle β

unreasonable (more than 10% variance from the observed values in Table 1 or outside of the expected range for a parameter).

Because of the large uncertainty of the values of parameters $h_o$ and $\varepsilon^c$ in some of the calculations the values of these parameters were modified to to determine what values were needed to obtain agreement within about 10% error of the performance parameters (Q, $h_c$, and L).

The mud depth $h_o$ directly affected the static pressure driving the flow through the cake. The $h_o$ value was increased until the calculated flow rate matched the experimental flow rate. This resulted in unreasonable values of $h_o$ (more than 10% increase over the Table 1 value) for all three experiments. The cake porosity was not measured though it was expected to fall in the range discussed previously. The values of $\varepsilon^c$ were changed from 0.45 to 0.55, the maximum value observed [14].

Changing $\varepsilon^c$ did not increase the calculated flow rate to an acceptable value (within 10% of the experiment value) for each experiment. By increasing $h_o$ by less than 10% from Table 1 value, along with changing $\varepsilon^c$ the flow rates could be exactly matched for Experiments 1 and 2. To achieve an acceptable flow rate in Experiment 3, $h_o$ needed to be increased to an unreasonable value and the length of mud L on the screen exceeded the total screen length (2.4m) for the shaker.

Overall, the results in Table 2 show in the case of Experiments 1 and 2 the parameters $h_o$ and $\varepsilon^c$ could be varied within a plausible range to show the model can reasonably match the observed experimental data. However, improved measurements are needed to verify these results.

Fig. 2 shows a plot of the calculated cake height as a function of position along the screen as calculated for Experiment 1 with $\varepsilon^c = 0.55$. The figure also shows the position of the screen relative to the horizontal axis and the position of the mud height. The plot is not to scale causing the

International Journal of Engineering Research & Technology (IJERT)
ISSN: 2278-0181
Vol. 6 Issue 02, February-2017

3 deg slope of the screen to appear larger than actual. As expected, the cake height starts at zero (at the screen surface) and gradually increases to the final cake height above the screen at the point where the mud and cake curves intersect.

Comparison of the model calculations with experimental data show the model under predicted the liquid flow rate based on the parameter values input to the model. Parameters, such as the cake porosity, were not accurately known for the experiments but were estimated for packed beds. Some aspects

Table 1. Experimental data for the 1 meter wide Mongoose Shale Shaker.

| PARAMETER | | UNITS | Expt 1 | Expt 2 | Expt 3 |
|---|---|---|---|---|---|
| MODEL INPUT | Number of gravity accelerations due to vibrations, $G_{max}$ | - | 10.24 | 6.22 | 2.59 |
| | Deck angle, β | deg | 3 | 3 | 3 |
| | Average particle size, $d_p$ | m | 0.0004 | 0.0004 | 0.0003 |
| | Mass fraction of sand in the mud | % (wt/wt) | 13.55 | 13.55 | 13.3 |
| | Volume fraction of Liquid in the mud, $\varepsilon^m$ | - | 0.938 | 0.938 | 0.939 |
| | Volume fraction of Liquid in the cake, $\varepsilon^c$ | - | 0.45 | 0.45 | 0.45 |
| | Volume fraction of clay in the liquid | - | 0.036 | 0.036 | 0.036 |
| | Colloidal Liquid Properties:<br>Bulk density, $\rho^L$<br>Plastic Viscosity, $\mu_o$<br>Yield Stress, $\tau_o$<br>Surface Tension, $\sigma$ | <br>$kg\ m^{-3}$<br>$kg\ m^{-1}s^{-1}$<br>$N\ m^{-2}$<br>$N\ m^{-1}$ | <br>1090<br>0.00123<br>0.037<br>0.0728 | <br>1090<br>0.0012<br>0.037<br>0.0728 | <br>1102<br>0.0012<br>0.037<br>0.0728 |
| | Screen properties:<br>Thickness, $h^{scr}$<br>Permeability, $k^{scr}$<br>Pososity, $\varepsilon^{scr}$ | <br>m<br>$m^2$<br>- | <br>0.000422<br>$2.73 \times 10^{-9}$<br>0.7 | <br>0.000422<br>$2.73 \times 10^{-9}$<br>0.7 | <br>0.000422<br>$2.73 \times 10^{-9}$<br>0.7 |
| OBSERVED | Liquid flow rate through the screen, $Q$ | $m^3\ s^{-1}$ | 0.0507 | 0.0462 | 0.0398 |
| | Velocity of cake moving across screen, $v_x^c$ | $m\ s^{-1}$ | 0.305 | 0.251 | 0.056 |
| | Depth of mud above the screen at inlet, $h_o$ | m | 0.110 | 0.112 | 0.166 |
| | Qualitative Observations | Surface was turbulent, ranged from 0.1 to 0.2 m | | | |
| | Length of Mud above cake, $L$ | m | 1.1 - 1.9 | 1.3 - 2.0 | 2.0 - 2.3 |
| | Observations | Edge of the mud was irregular and fluctuated | | | |
| | Cake Height at end of screen | m | 0.01 - 0.03 | 0.01 - 0.03 | > 0.3 |
| | Observations | Tended to be flat with some irregularity, not measured directly | | | |

International Journal of Engineering Research & Technology (IJERT)
ISSN: 2278-0181
Vol. 6 Issue 02, February-2017

**Table 2**. Calculation results. The "Table 1" rows list the values from Table 1 for each experiment. The remaining rows show the model calculated values of ($Q$, $h_c$, and $L$) for comparison with the experiments and show theinput values of the cake porosity and mud height used in the calculations. In some of the calculations the input values were modified to obtain agreement between the experiment and calculated values of $Q$, $h_c$, and $L$. The shaded values were unreasonable, more than about 10% variation from the observed experimental values.

| | Values observed in experiments to be compared with model calculations | | | Input values to model from experiment or modified | |
|---|---|---|---|---|---|
| | $Q$ x $10^2$ m$^3$ s$^{-1}$ | $h_c$ x $10^2$ m | $L$ m | $\varepsilon^c$ | $h_o$ m |
| Table 1 Expt 1 Values | 5.07 | 0.1 to 0.3 | 1.1 – 1.9 | 0.45 | 0.110 |
| | Calculated Values | | | Model Input Values | |
| Model Calculations Expt 1 | 2.69 | 1.12 | 1.88 | 0.45 | 0.110 |
| | 5.07 | 2.11 | 3.14 | 0.45 | 0.186 |
| | 3.77 | 1.97 | 1.72 | 0.55 | 0.110 |
| | 3.43 | 1.43 | 1.83 | 0.45 | 0.110 |
| | 4.72 | 2.47 | 1.63 | 0.55 | 0.110 |
| | 5.06 | 2.66 | 1.75 | 0.55 | 0.118 |
| | $Q$ x $10^2$ m$^3$ s$^{-1}$ | $h_c$ x $10^2$ m | $L$ m | $\varepsilon^c$ | $h_o$ m |
| Table 1 Expt 2 Values | 4.62 | 0.1 to 0.3 | 1.1 – 2.0 | 0.45 | 0.112 |
| | Calculated Values | | | Model Input Values | |
| Model Calculations Expt 2 | 2.51 | 1.27 | 1.89 | 0.45 | 0.112 |
| | 4.63 | 2.34 | 3.10 | 0.45 | 0.186 |
| | 3.51 | 2.24 | 1.71 | 0.55 | 0.112 |
| | 3.18 | 1.61 | 1.83 | 0.45 | 0.112 |
| | 4.36 | 2.78 | 1.61 | 0.55 | 0.112 |
| | 4.63 | 2.94 | 1.70 | 0.55 | 0.119 |
| | $Q$ x $10^2$ m$^3$ s$^{-1}$ | $h_c$ x $10^2$ m | $L$ m | $\varepsilon^c$ | $h_o$ m |
| Table 1 Expt 3 Values | 3.98 | > 0.3 | 2.0 to 2.3 | 0.45 | 0.166 |
| | Calculated Values | | | Model Input Values | |
| Model Calculations Expt 3 | 1.49 | 3.33 | 2.53 | 0.45 | 0.166 |
| | 3.98 | 8.87 | 5.98 | 0.45 | 0.402 |
| | 2.08 | 5.84 | 2.05 | 0.55 | 0.166 |
| | 1.72 | 3.82 | 2.44 | 0.45 | 0.166 |
| | 2.33 | 6.51 | 1.92 | 0.55 | 0.166 |
| | 3.58 | 10.0 | 2.95 | 0.55 | 0.258 |

of the physics are not fully understood, including how the vibrations cause the cake porosity to increase and how the vibrations cause the liquid to detach from the bottom surface of the screen.

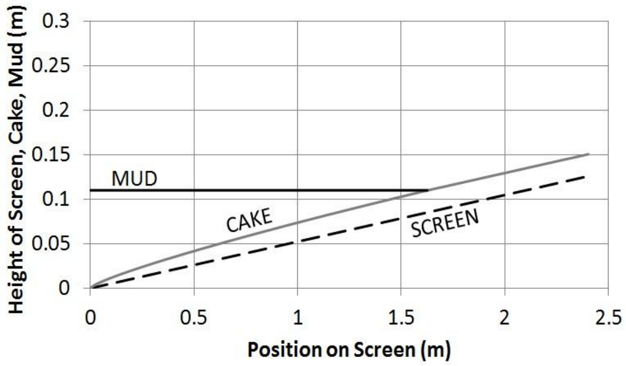


Figure 2. Cake height for the Experiment 1 with modified values of $\varepsilon^c = 0.55$.

By increasing the cake porosity above that for a loose packed bed, but still within the range observed in pilot tests, the model calculations can approach (within 10% or less error) the observed experimental flow rates. The model calculated cake height profiles similar to those expected from qualitative observations of the full scale shaker.

## IV. CONCLUSIONS

Model calculations of a shaker based on continuum mechanics were compared to experimental data from a Mongoose shale shaker. With cake porosity of 0.55 the model calculations compared well with two of the three experiments. For the third experiment, the calculated model parameters were outside of the expected range for the parameters. The profile shape of the calculated cake height was consistent with the model assumptions and experimental observations. Future work should improve and expand measurements, particularly those of the cake porosity and the inlet mud height.

### Symbols

| | | |
|---|---|---|
| b | [m] | shaker width |
| $d_p$ | [m] | average particle size |
| $f$ | [-] | friction factor |
| $F_z$ | [N] | drag force |
| $g$ | [m s$^{-2}$] | gravity acceleration |
| $G_{max}$ | [-] | number of gravities |
| $h_0$ | [m] | depth of mud above the screen at inlet |
| $h_c$ | [m] | cake height |
| $h_{sc}r$ | [m] | screen thickness |
| $k_{scr}$ | [m$^2$] | screen permeability |
| $H_e$ | [-] | Hedstrom Number |
| $L$ | [m] | screen length |
| $P$ | [Pa] | pressure |
| $R$ | [m] | effective pore radius |
| $R_e$ | [-] | Reynolds number |
| $U$ | [m s$^{-1}$] | velocity within the pores |
| $V$ | [m s$^{-1}$] | face velocity of liquid through the cake |
| $v_x^c$ | [m s$^{-1}$] | velocity of the cake |
| $Q$ | [m3 s$^{-1}$] | liquid flow rate |
| Greek symbols | | |
| $\beta$ | [deg] | deck angle |
| $\mu_o$ | [kg m$^{-1}$. s$^{-1}$] | plastic viscosity of the liquid |
| $\tau_o$ | [N m$^{-1}$] | yield stress |
| $\rho$ | [kg m$^{-1}$] | liquid bulk density |
| Sub- and Superscripts | | |
| c | | quantities for the cake |
| m | | quantities for the mud |
| scr | | quantities for the screen |
| S | | solid |
| L | | liquid |
| x,z | | vector components in the x and z directions |
| atm | | atmospheric |

## REFERENCES

[1] Wojtanowicz, A. Environmental control potential of drilling engineering: An overview of existing technologies. in SPE/IADC Drilling Conference. 1991. Society of Petroleum Engineers.
[2] Wojtanowicz, A., Environmental control of drilling fluids and produced water, in Environmental technology in the oil industry. 2016, Springer. p. 101-165.
[3] Committee, A.S.S., Drilling fluids processing handbook. 2011: Elsevier.
[4] Delaney, G.W., Cleary, P.W., Hidden, M., Morrison, R.D., Testing the validity of the spherical DEM model in simulating real granular screening processes. Chemical engineering science, 2012. 68(1): p. 215-226.
[5] Hoberock, L., A study of vibratory screening of drilling fluids. Journal of Petroleum Technology, 1980. 32(11): p. 1,889-1,902.
[6] Lal, M. and L. Hoberock, Solids-conveyance dynamics and shaker performance. SPE drilling engineering, 1988. 3(04): p. 385-394.
[7] Brundrett, E., Prediction of pressure drop for incompressible flow through screens. Journal of fluids engineering, 1993. 115(2): p. 239-242.
[8] Fowler, R. and S. Lim, The influence of various factors upon the effectiveness of separation of a finely divided solid by a vibrating screen. Chemical Engineering Science, 1959. 10(3): p. 163-170.
[9] Armour, J.C. and J.N. Cannon, Fluid flow through woven screens. AIChE Journal, 1968. 14(3): p. 415-420.
[10] Weibing, Z., D. Chengzhong, and W. Heshun, Kinematic law of solids on a drilling fluid vibrating screen. Petroleum Science and Technology, 2013. 31(16): p. 1608-1616.
[11] Raja, V., Chase, G.G., Jones, B.N., Geehan, T., Continuum model predicts shale shaker performance. World oil, 2011. 232(6).
[12] Mueller, S., E. Llewellin, and H. Mader. The rheology of suspensions of solid particles. in Proceedings of the Royal

International Journal of Engineering Research & Technology (IJERT)
ISSN: 2278-0181
Vol. 6 Issue 02, February-2017

Society of London A: Mathematical, Physical and Engineering Sciences. 2009. The Royal Society.
[13] Foust, A.S., Wenzel, L.A., Clump, C.W., Maus, L., Andersen, L.B., Principles of unit operations. 2008: John Wiley & Sons.
[14] Raja, V., Shale Shaker Model and Experimental Validation. 2012, University of Akron.
[15] Chase, G.G., Dachavijit, P., A correlation for yield stress fluid flow through packed beds. Rheologica acta, 2005. 44(5): p. 495-501.
[16] Bird, R.B., Stewart., W.E., Lightfoot, E.N., Transport phenomena. 2nd. New York, 2002.
[17] Ruth, B., Studies in filtration III. Derivation of general filtration equations. Industrial & Engineering Chemistry, 1935. 27(6): p. 708-723.
[18] Teoh, S.K., Tan, R., Tien, C., Analysis of cake filtration data—a critical assessment of conventional filtration theory. AIChE journal, 2006. 52(10): p. 3427-3442.
[19] Smiles, D., A theory of constant pressure filtration. Chemical Engineering Science, 1970. 25(6): p. 985-996.
[20] Chase, G.G., Mayer, E., Filtration. Kirk-Othmer Encyclopedia of Chemical Technology, 2003.
[21] Chase, G.G., Willis, M.S., Compressive cake filtration. Chemical engineering science, 1992. 47(6): p. 1373-1381.
[22] Willis, M.S., Tosun, I ., A rigorous cake filtration theory. Chemical Engineering Science, 1980. 35(12): p. 2427-2438.
[23] Lee, J.H., Bang, K.W., Characterization of urban stormwater runoff. Water Research, 2000. 34(6): p. 1773-1780.
[24] Slattery, J.C., Momentum, energy, and mass transfer in continua. McGraw-Hill chemical engineering serie, 1972.
[25] Willis, M.S., Tosun, I., Choo, W., Chase, G.G., Desai, F., A dispersed multiphase theory and its application to filtration. Advances in Porous Media, 1991. 1: p. 179-294.
[26] Hanks, R.W., Dadia, B.H., Theoretical analysis of the turbulent flow of non-Newtonian slurries in pipes. AIChE Journal, 1971. 17(3): p. 554-557.
[27] Constantinides, A ., Mostoufi , N., Numerical methods for chemical engineers with MATLAB applications. Vol. 443. 1999: Prentice Hall PTR Upper Saddle River, NJ.
[28] Davis, M.E., Numerical methods and modeling for chemical engineers. 2013: Courier Corporation.

International Journal of Engineering Research & Technology (IJERT)
ISSN: 2278-0181
Vol. 6 Issue 02, February-2017

## APPENDIX: MODEL DESCRIPTION

The shaker is modeled as a continuous cake filtration. The cake forms as particles collect on the cake surface while the vibrations move the cake across the screen. The process is steady when the formation rate equals the of removal rate. Cake filtration models are reported in literature [17-23].

A continuum model approach here applies to either Newtonian or yield stress liquid rheology. Constitutive expressions account for liquid flow drag forces in the cake to obtain mathematical closure of the equations. The process is steady, isothermal, non-reacting, has constant material properties, and no phase change occurs. The flow drag on the cake particles dominates over the drag at the walls of the shaker channel. The particles are uniformly distributed in the mud and the cake is incompressible. Mass and momentum balances reduce to

Mass Balance:

$$\frac{\partial v_z^i}{\partial z} = 0 \text{ , } i = c, m \text{ hence } v_z^i = f(x) \qquad \text{(A1)}$$

$$\frac{\partial v_x^i}{\partial z} = 0 \qquad \text{hence} \qquad v_x^i = \text{constant} \qquad \text{(A2)}$$

Momentum Balance, z-component, Liquid phase:

$$0 = \varepsilon^i \frac{\partial P}{\partial z} + F_z^i - \varepsilon^i \rho^L g_z = 0 \qquad \text{(A3)}$$

The superscripts i =c, m, and scr indicate the quantities are for the cake, mud, or screen regions. The quantities $\varepsilon^i$ are the porosities (volume fractions occupied by the liquid phase) of the $i^{\text{th}}$ region, $v_j^i$ are the $j$ directional components of the velocity, and $F_j^i$ are the drag force components between the phases in the $i^{\text{th}}$ region.

### MASS JUMP BALANCE

At the cake-screen boundary the velocity of the solid phase in the vertical direction is zero. Combining this boundary condition with Eq.(A1) makes the cake vertical velocity zero everywhere. An expression relating the mud and cake velocities to the rate of change of cake height is obtained from the mass jump balance [24, 25]. Superscripts S and L indicate the sand or liquid phase components for clarity.

The jump balance applied to the differential section in Fig.3 becomes

$$[\varepsilon^{mL}\rho^L(-v_x^{mL}n_x - v_z^{mL}n_z) + \varepsilon^{ms}\rho^s(-v_x^{ms}n_x - v_z^{ms}n_z)]$$
$$= [\varepsilon^{cL}\rho^L(-v_x^{cL}n_x - v_z^{cL}n_z) + \varepsilon^{cs}\rho^s(-v_x^{cs}n_x)] \qquad \text{(A4)}$$

where $n_x$ and $n_z$ are unit direction vector in the x and z directions. The solid and liquid phases in Eq.(A4) are independently conserved, yielding

$$\varepsilon^{mL}\rho^L(v_x^{mL}n_x + v_z^{mL}n_z) = \varepsilon^{cL}\rho^L(v_x^{cL}n_x + v_z^{cL}n_z) \qquad \text{(A5)}$$

$$\varepsilon^{ms}\rho^S(v_x^{mS}n_x + v_z^{mS}n_z) = \varepsilon^{cs}\rho^s(v_x^{cS}n_x) \qquad \text{(A6)}$$

Neglecting particle settling in the mud gives

$$v_z^{mL} = v_z^{mS} \qquad \text{(A7)}$$

and a lack of separation mechanism in the x-direction gives

$$v_x^{iL} = v_x^{iS} \qquad \text{(A8)}$$

Equations (A5)-(A8) are combined

$$\frac{n_x}{n_z} = \left(\frac{1-\varepsilon^{mL}}{\varepsilon^{mL}-\varepsilon^{cL}}\right)\frac{\varepsilon^{cL}v_z^{cL}}{v_x^{cS}} \qquad \text{(A9)}$$

From geometric arguments, $n_x$ and $n_z$are given by

$$n_x = \frac{-\Delta h_c}{\sqrt{\Delta x^2 + \Delta h_c{}^2}} \qquad \text{(A10)}$$

$$n_z = \frac{\Delta x}{\sqrt{\Delta x^2 + \Delta h_c{}^2}} \qquad \text{(A11)}$$

Combining (A9)-(A11) in the limit as $\Delta x \rightarrow 0$, gives

$$\frac{dh_c}{dx} = -\left(\frac{1-\varepsilon^{mL}}{\varepsilon^{mL}-\varepsilon^{cL}}\right)\frac{V}{v_x^{cS}}$$

(A12)

where the face velocity $V = \varepsilon^{cL}v_z^{cL}$ is applied. The superscripts S and L are dropped from Eq.(A.12) to obtain Eq.(1).

Momentum Balance

The momentum balance controls the rate of liquid flow. The pressure $P_c$ at the top of the cake is obtained from the static head in the mud, as indicated in Fig.4.

$$P_c = P_{atm} + \rho^m g\,(h_m - h_c)$$

(A13)

The height from the screen to the surface of the mud, $h_m$, is determined from Fig.1.

$$h_m = h_o - x\,tan(\beta) \qquad \text{(A14)}$$

Integration of Eq.(A3) gives

$$P_c - P_{scr} = -\left(\frac{F_Z^c}{\varepsilon^c} + \rho^L g\right)h_c \qquad \text{(A15)}$$

$$P_{scr} - P_o = -\left(\frac{F_Z^{scr}}{\varepsilon^{scr}} + \rho^L g\right)h_{scr} \qquad \text{(A16)}$$

Combining Eqs. (A13), (A15)-(A16), gives

$$\left(\frac{F_Z^c}{\varepsilon^c}h_c + \frac{F_Z^{scr}}{\varepsilon^{scr}}h_{scr}\right) + [\rho^m(h_m - h_c) + \rho^L(h_c + h_{scr})]g = 0$$

(A17)

where $\rho^m$ is the bulk density of the mud

$$\rho^m = \varepsilon^m\rho^L + (1-\varepsilon^m)\rho^S$$

(A18)

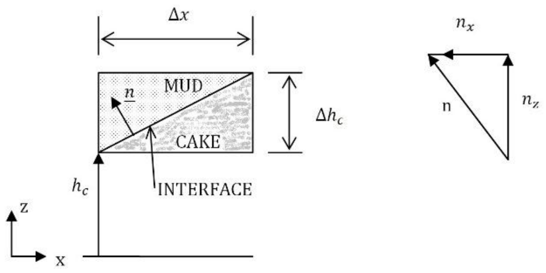


Figure 3. Section of the interface between the mud and the cake regions.

Drag and Friction Factor

The drag forces in Eq.(A17) are modeled in terms of friction factors. The drag force through the cake is given by

$$F_Z^c = -\frac{3(1-\varepsilon^c)}{\varepsilon^{c^2}d_p}\rho^L|V|Vf^c$$

(A19)

For a yield stress fluid the friction factor $f^c$ is [15]

$$f^c = 5.741 R_{ep}^{-1.969} H_{ep}^{0.958} + \frac{60}{R_{ep}} + 0.6$$
(A20)

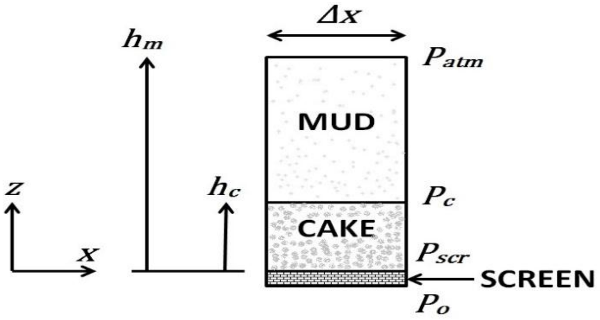


Figure 4. A section of the screen of length $\Delta x$, cake of height $h_c$ and mud height $h_m$ at an arbitrary position of x.

where

$$R_{ep} = \frac{\rho^L d_p |V|}{\mu_o (1-\varepsilon^c)}$$
(A21)

$$H_{ep} = \frac{\tau_o \rho^L d_p^2}{\mu_o^2} \left(\frac{\varepsilon^c}{1-\varepsilon^c}\right)^2$$
(A22)

and $\mu_o$ is the plastic viscosity and $\tau_o$ is the yield stress.

For the yield stress flow through the screen a similar friction factor correlation is not available but a relation can be derived for a bundle of tubes of radius $R$ and length $L$. The Fanning Friction factor correlation derived by Hanks and Dadia [26] for the for flow in a tube with average velocity $U = \frac{V}{\varepsilon^{scr}}$ is applied, where

$$R_e = \frac{\rho^L |V|\, 2R}{\varepsilon^{scr} \mu_o}$$
(A23)

$$H_e = \frac{\tau_o \rho^L\, 4R^2}{\mu_o^2}$$
(A24)

The correlation is assumed to have the form

$$f = f_o + f_\infty$$
(A25)

where $f_o$ is the asymptotic solution for ${R_e}^2 \ll H_e$ and $f_\infty$ for ${R_e}^2 \gg H_e$. For the latter,

$$f_\infty = \frac{16}{R_e} + 0.001$$
(A26)

where the 0.001 artificially places a lower bound on the value of the friction factor (and helps in the mathematics to avoid zero-divide) for large $R_e$.

The correlation for $f_o$ has the assumed form

$$f_o = c_1 R_e^{c_2} H_e^{c_3}$$
(A27)

The coefficients $c_1 = 3.83 \pm 0.68$, $c_2 = -1.83 \pm 0.04$, and $c_3 = 0.87 \pm 0.02$ were obtained by least-squares-error fitting of 20 random points from the friction factor plot in Hanks and Dadia [26]. Hence, the friction factor is approximated by

$$f^{scr} = 3.83 R_e^{-1.83} H_e^{0.87} + \frac{16}{R_e} + 0.001 \qquad \text{(A28)}$$

The drag force through the screen is related to the friction factor by

$$F_z^{scr} = -\frac{1}{R\varepsilon^{scr}} \rho^L |V| V f^{scr} \qquad \text{(A29)}$$

Combining laminar flow in a tube with Darcy's law for porous medium gives the effective pore radius as

$$R = \sqrt{\frac{8k_{scr}}{\varepsilon^{scr}}} \qquad \text{(A30)}$$

## BOUNDARY AND FLOW CONDITION

Boundary condition $h_c = 0$ at x=0 is applied to integrate Eq.(A12). The liquid flows through the cake when several criteria are satisfied. First the mud height must exceed the cake height, $h_m > h_c$. Second, the static pressure must exceed the capillary pressure and the resistance due to the yield stress in the porous media and the pores in the screen [15]

$$[\rho^m (h_m - h_c) + \rho^L (h_c + h_{scr})] g > 10.5 \frac{\tau_o (1-\varepsilon^C)}{d_p \varepsilon^c} h_c$$
(A31)

$$[\rho^m (h_m - h_c) + \rho^L (h_c + h_{scr})] g > 2 \frac{\tau_o}{R} h_{scr}$$
(A32)

Here, height $h_m$ is at an arbitrary position of x.

To solve Eq.(A12) for the cake height $h_c$, a second order accurate implicit Euler method [27, 28] was applied. The liquid velocity was numerically integrated over the surface of the screen to obtain the liquid flow rate.